



HAL
open science

Three octave visible to mid-infrared supercontinuum generation seeded by multimode silica fiber pumped at 1064 nm

Y. Leventoux, Yago Arosa Lobato, Geoffroy Granger, Idris Tilouine, K. Krupa, A. Tonello, V. Couderc, S. Février

► To cite this version:

Y. Leventoux, Yago Arosa Lobato, Geoffroy Granger, Idris Tilouine, K. Krupa, et al.. Three octave visible to mid-infrared supercontinuum generation seeded by multimode silica fiber pumped at 1064 nm. *Optics Letters*, 2023, 48 (17), pp.4582. 10.1364/OL.497678. hal-04650175

HAL Id: hal-04650175






<https://hal.science/hal-04650175v1>

Submitted on 16 Jul 2024

HAL is a multi-disciplinary open access archive for the deposit and dissemination of scientific research documents, whether they are published or not. The documents may come from teaching and research institutions in France or abroad, or from public or private research centers.

L'archive ouverte pluridisciplinaire **HAL**, est destinée au dépôt et à la diffusion de documents scientifiques de niveau recherche, publiés ou non, émanant des établissements d'enseignement et de recherche français ou étrangers, des laboratoires publics ou privés.

Three octave visible to mid-infrared supercontinuum generation seeded by multimode silica fiber pumped at 1064 nm

Y. LEVENTOUX,^{1,*}  G. GRANGER,¹ Y. AROSA,^{1,2} I. TILOUINE,¹ K. KRUPA,³  A. TONELLO,¹  V. COUDERC,¹  AND S. FÉVRIER¹ 

¹ Université de Limoges, XLIM, UMR CNRS 7252, 123 Av. A. Thomas, 87060 Limoges, France

² Departamento de Física Aplicada, Univ. de Santiago de Compostela, 15705 Santiago de Compostela, Spain

³ Institute of Physical Chemistry, Polish Academy of Sciences, Warsaw, ul. Kasprzaka 44/52, 01-224, Poland

*yann.leventoux@gmail.com

Hyperspectral spectroscopy requires light sources with wide spectral ranges from the visible to the mid-infrared. Here, we demonstrate the first fiber-based mid-infrared supercontinuum covering three octaves of frequency by leveraging 1- μm laser technology. The process consists in spectral broadening of a 1064-nm pump toward 0.48–2.5 μm in a graded-index multimode fiber, followed by a fluoro-indate fiber used to reach deeper into the near infrared (4.3 μm). Finally, an arsenic selenide chalcogenide fiber allows us to reach the 6- μm wavelength region, providing a 0.75–6- μm supercontinuum. We illustrate the potential of this light source by recording mid-infrared absorption spectra of organic compounds. © 2023 Optica Publishing Group

<https://doi.org/10.1364/OL.497678>

Light–matter interactions are routinely used to characterize materials and biological samples across a large range of spectral windows [1–3]. Visible and near-infrared (NIR) light (from 400 nm to 2.5 μm) probes electronic transitions in materials, providing information regarding bandgap, defects, and energy transfer, which is crucial for the semiconductor and optoelectronic industries, and for understanding complex processes such as photosynthesis [4–6]. At lower photon energies, the middle-wave infrared (mid-IR) light (from 2.5 to 28 μm) excites molecular vibrational modes and provides rich chemical and structural information useful for material identification. Furthermore, the Earth’s atmosphere exhibits several windows of relatively high transparency, around 1.55 μm , from 3 to 5 μm , and from 8 to 12 μm , making these spectral ranges ideal for remote sensing applications such as high-resolution molecular spectroscopy, monitoring of atmospheric pollutants, highly sensitive biological and chemical molecular identification in industrial processes, and defense fields, to name a few [7,8]. The recent images of the early universe taken by the James Webb space telescope confirmed the broad interest for the mid-IR spectral range [9]. With the aim of achieving similar breakthroughs, researchers design high-resolution mid-IR spectrometers, which need to be precisely calibrated by means of artificial sources mimicking

star light [10]. The rising popularity of these high-precision applications has sparked intense research in the generation of supercontinuum (SC) sources that can produce intense and broadband light, spanning several octaves of frequency from the visible to the mid-IR, with excellent beam quality.

In our previous work, we have developed a Watt-level mid-IR SC by pumping a single-mode fluoride glass fiber by means of an amplified ultrafast thulium-doped fiber oscillator and demonstrated its suitability for high spatial resolution spectro-microscopy. The spectral coverage spanning only one octave from 2 to 4.3 μm was well suited to spectroscopic studies of the vibrational resonances of the -CH- group but precluded the studies across the fingerprint region [11]. Indeed, the pump wavelength of 2 μm lying in the large anomalous dispersion regime of the nonlinear fiber mode hinders the extension of the spectrum toward shorter wavelengths, while the phonon energy of the fluoride glass forbids nonlinear frequency conversion toward wavelengths longer than approximately 4.3 μm . One of the strategies to obtain spectra spanning from the visible/NIR to the mid-IR consists in pumping nonlinear materials with lower phonon energies, to reach further in the infrared, by means of shorter wavelength sources. This strategy is implemented by means of a cascaded fiber system. For example, Venck *et al.* generated first a 0.7–4.1- μm SC in fluoride fiber pumped by a telecom-grade picosecond erbium-doped fiber laser [12]. Solitons generated and frequency shifted by the intra-pulse stimulated Raman scattering in the fluoride fiber were then launched into an arsenic selenide chalcogenide glass fiber to further extend the SC up to 10 μm . In this implementation of the concept of a cascaded fiber laser system, the visible and near-infrared portions of the generated spectra were filtered out to avoid deterioration of the chalcogenide fiber through the multiphoton absorption processes, resulting in a still impressive 2–10- μm fiber SC. Similarly, we recently proposed an alternative approach using a shorter wavelength pump based on ytterbium technology to cover the visible/NIR part of the spectrum in a silica fiber, followed by a fluoro-indate (InF₃) fiber to extend the spectrum up to approximately 3.4 μm [13]. We initiated the SC generation in a telecom-grade graded index multimode fiber (GIMF)

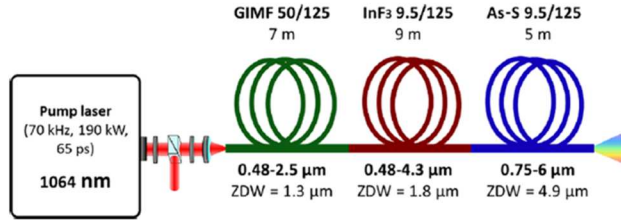


Fig. 1. Scheme of the experimental setup for SC generation. The fibers are butt-coupled.

by exploiting the rich nonlinear spatiotemporal dynamics in GIMF originated from the periodic longitudinal beating of the different propagating modes. We have shown that among these novel effects, nonlinear beam cleaning and geometric parametric instabilities (GPIs) play a key role in enhancing the nonlinear frequency conversion involved in SC generation [14–20]. Beam cleaning allows, from a multimode pump wave, for obtaining a quasi-single mode propagation in the GIMF either on the pump wave itself, with the Kerr beam self-cleaning [17,18], or on the Raman frequencies, through the Raman beam cleanup [21,22]. The Kerr beam cleaning effect, by increasing the power spatial density at the pump wavelength, decreases the threshold for the appearance of subsequent nonlinear effects such as GPI, a process based on intermodal four-wave mixing, which generates new frequency components far detuned from the pump by hundreds of THz [15,23]. Previous research has shown that GPI can provide pump conversion over a wide spectral range, from visible to infrared wavelengths depending on the pump frequency and the opto-geometrical parameters of the GIMF. We have shown in Ref. [13] that the 1.9- μm GPI Stokes sideband generated by pumping a GIMF with 1064-nm nanosecond pulses can be amplified in a thulium-doped fiber amplifier and subsequently broadened in an InF_3 fiber. Using this approach, we generated an SC spanning one octave from 1.7 to 3.4 μm . In another implementation, Raman-induced effects, such as Raman beam cleanup and soliton self-frequency shift (SSFS) using a pump wave at 1 μm , allow for generating spectra of high power spectral density and high brightness from the visible to approximately 2.5 μm , the transparency limit of silica glass fibers [14,16]. Here, we demonstrate the first fiber-based mid-IR SC covering three octaves of frequency by leveraging the 1- μm laser technology.

Figure 1 shows schematically our experimental setup based on the free-space injection of a laser beam into a cascade of butt-coupled fibers. The various fibers were butt-jointed via three-dimension translation stages. We use a modified Spark SIRIUS laser system that delivers pulses with 65-ps duration, 1064-nm wavelength, and 70-kHz repetition rate as a pump. Its input peak power is adjustable, up to 190 kW (12 μJ per pulse) by means of a polarizing beam splitter and two half-wave plates, which also determine the orientation of linear polarization. A 6.5- μm radius ($@1/e^2$) Gaussian laser beam is launched into a 7-m-long GIMF with 50- μm core diameter and 0.2 numerical aperture. The calculated zero dispersion wavelength (ZDW) for this fiber is 1.27 μm . We tried to match the size of the input beam to that of the fundamental LP_{01} mode of the fiber ($w_0^{\text{LP}_{01}} = 6 \mu\text{m} @1/e^2$) to excite a low number of modes while maximizing the coupling efficiency ($\sim 85\%$). Then, the GIMF was butt-coupled to a 9-m-long piece of InF_3 fiber, with a core diameter of 9.5 μm , a numerical aperture of 0.3, and a ZDW calculated at 1.8

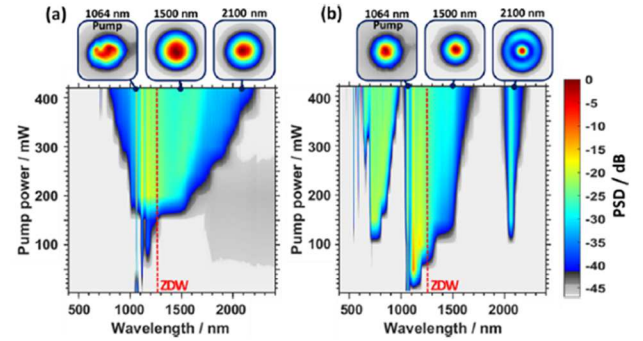


Fig. 2. Spectral evolution of the beam at the GIMF output as a function of average pump power for launching conditions leading to (a) inhibited or (b) maximized GPI. Insets show the spatial distribution of energy for various wavelengths.

μm . Finally, the fluoride fiber was butt-coupled to a 5-m-long piece of As-S chalcogenide fiber with a core diameter of 9.5 μm , a numerical aperture of 0.3, and a ZDW calculated at 4.9 μm . The lengths of InF_3 and As-S fibers have not been optimized, suggesting that potential adjustments might enhance the final supercontinuum extension. Due to nonlinear propagation and multiphoton absorption, only 50% of the energy is transmitted through the GIMF, at maximum input power. The transmission coefficients are 25% between GIMF and InF_3 fiber, and 30% between InF_3 fiber and As-S fiber. Improvements might be achieved using mode field adaptors or by splicing the fibers. The spectrum was recorded for each fiber output along with the pump wave. We used two spectrum analyzers covering the spectral bands of 0.35–1.7 μm and 1.5–3.5 μm , respectively, as well as a monochromator that can measure light up to 20 μm . In addition, we used a spatial/spectral measurement device developed in-house to obtain the evolution of the beam profile at the output of the GIMF as a function of wavelength, since the knowledge of the spatial distribution of energy is instrumental in understanding the mechanisms of nonlinear spectral conversion in a multimode fiber [13].

The first series of experiments consisted in determining which nonlinear dynamical process, either Raman or GPI, leads to a maximized SC extension. It is worth noting that the GPI's efficiency is highly dependent on the dynamics of the self-imaging, and thus on the number of modes initially excited. Thus, it is possible to control the magnitude of the GPI sidebands by varying the input conditions (namely polarization orientation and power). To analyze Raman and GPI contributions separately, we have studied two cases: one with GPI sidebands inhibited and a second case where GPI sidebands are maximized. In the scenario with suppressed GPI, an extinction of approximately 50 dB was estimated. For both cases, we have measured the spectrum as a function of the average power. The results are presented in Fig. 2(a) when GPI are inhibited and in Fig. 2(b) when GPI is maximized. To avoid any spatial filtering by the collection optics, the spectrum was measured directly at the output of the GIMF, with a resolution of 0.1 nm. It is worth noting that the launching conditions that maximize GPI also decrease the laser induced damage threshold of the fiber, thereby limiting the pump power for this measurement to 90 kW. However, we were able to increase the pump power up to 190 kW when Raman-induced effects have a dominant role. The insets correspond to the near-field images of the fiber output beam at various relevant

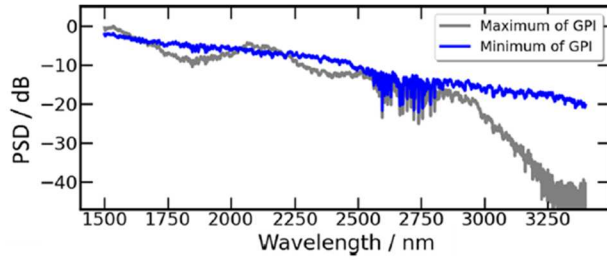


Fig. 3. NIR spectrum at the output of the InF₃ in both configurations at 90-kW pump power.

wavelengths. From Fig. 2(a), we observe how, as the power of the pump wave increases, the energy is transferred to the stimulated Raman scattering (SRS) Stokes sidebands at 1116 nm and 1174 nm, characteristic of silica glass (Raman shift $\Delta f = 13.2$ THz). When the power increases, the spectral generation reaches the solitonic regime of the fiber, which triggers SC generation up to 2200 nm. The near-field image of the pump wave at 1064 nm shows a concentrated, but clearly not Gaussian, spatial energy distribution, which is the signature of some multimodal content. In contrast, the Raman wavelengths strongly approach the fundamental mode due to Raman beam cleanup.

However, the results plotted in Fig. 2(b), obtained when the pump beam is nearly Gaussian, are in striking contrast with those of Fig. 2(a). We observe the appearance of two intense spectral lines at 730 nm and 2100 nm, both carrying a peak power near 20 kW, which are the signatures of the GPI. The pump wave still generates a Raman cascade up to 1700 nm. The insets in Fig. 2(b) show the spatial distribution of light at the output of the GIMF at three different wavelengths. The pump wave preserves its Gaussian profile even though it is not strictly single mode. As shown in Ref. [13], the GPI Stokes sideband is carried mainly by an LP₀₂ mode, which will finally lead to a poor injection efficiency in the following InF₃ single-mode fiber. To determine the process that maximizes the extension of the final SC, we analyze the impact of launching the GPI or SSFS signals into the InF₃ fiber constituting the second stage. By evaluating their effects, we aim to identify the most effective process for achieving optimal SC extension. Figure 3 shows the power spectral density recorded at the output of the InF₃ fiber for both cases. We observe that using GPI as a precursor, the SC reaches 3.2 μm , while the SSFS-seeded continuum exceeds 3.4 μm , the limit of the window of the spectrum analyzer used. Therefore, favoring solitonic and Raman effects in the graded-index multimode fiber is the most efficient way to extend the supercontinuum toward the mid-IR in the fluoro-iodate fiber. It is worth noting that Fig. 3 was plotted for 90 kW of peak power launched into the GIMF. However, when favoring the Raman effects, we were able to launch the maximal pump power available from the laser used (190 kW), without degradation of the fiber facet. In this configuration, the power spectral density (PSD) was measured at full power at the output of the GIMF and plotted in Fig. 4 (green curve). The spectrum at the output of the GIMF stops at 2.5 μm , the limit of transparency of silica. The spectrum was then recorded at full power at the output of the InF₃ fiber by means of the monochromator and plotted in Fig. 4 (blue curve). The proper combination of the GIMF and the InF₃ fiber allowed us to extend the spectrum from 470 nm to 4.3 μm with 1.4 μJ of energy corresponding to approximately 100 mW of average power. The sudden stop of the spectral broadening was attributed to the increase of the

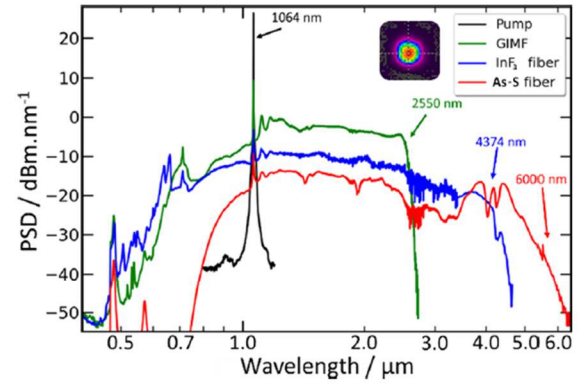


Fig. 4. Spectra measured at the output of the laser (black), the GIMF (green), the InF₃ fiber (blue), and the As-S fiber (red). Inset shows the near-field image of the beam at the InF₃ output.

effective area of the fundamental mode of the InF₃ fiber with wavelength, and the consequent decrease of the power spatial density. To increase the spectral coverage of the light source, we added a third stage using a highly nonlinear As-S chalcogenide glass fiber. The spectrum plotted in red extends from 750 nm to 6.3 μm with 400 nJ of energy, corresponding to approximately 30 mW of average power. It is worth noting that the mid-IR fibers display a few-mode behavior at wavelengths shorter than 3.7 μm , which might degrade the beam quality. However, proper launching conditions ensure quasi-single-mode operation, as shown in the inset to Fig. 4. We also observe that in our all-fibered architecture, light from 470 nm to 750 nm is absorbed by the As-S fiber. The development of broadband wavelength splitters made of fluoride fibers could potentially help to preserve the visible part of the spectrum, thereby extending the spectral coverage through more than one decade of frequency.

High-power mid-IR SC has great potential application in the identification and quantification of molecular compounds by molecular infrared absorption spectroscopy (IRS), which benefits from the broadband SC source. IRS is used to determine the different chemical functional groups present in a sample by analyzing characteristic absorbed frequencies in the mid-infrared. As a test for our SC source, we measured the absorption spectra of ethanol and paraffin sandwiched in between two microscope slides. The thickness of the sample was in the range of 500 μm . The samples were placed in the collimated beam of the InF₃ fiber. The transmitted spectra were recorded with and without the sample. Then, we deduced the absorption spectrum by subtracting the two spectra. We repeated this procedure for the two materials and the results are reported in Fig. 5. These spectra allow to clearly identify the wavelengths corresponding to the molecular vibrations of the chemical groups of the molecules studied. It is possible to see for ethanol [C₂H₅OH (Fig. 5(a)), the response of the alkyl group -CH₃, methylene group -CH₂-, and hydroxyl group -OH]. For paraffin C₁₂H₂₆ [Fig. 5(b)], the spectrum shows absorption lines for the alkyl group -CH₃ and the methylene group -CH₂-. Reference spectra from NIST [24] are also plotted for comparison, demonstrating that our measurements align with the standards. The absorption peaks match in position, with magnitude variations attributable to differences in concentration (for ethanol) and phase (for paraffin).

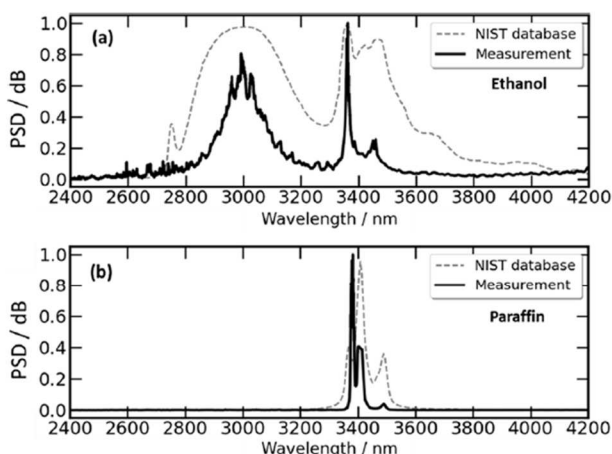


Fig. 5. Absorption spectra of (a) ethanol (C_2H_5OH) and (b) paraffin ($C_{12}H_{26}$) thin films. Dashed lines represent the NIST reference spectra extracted from Ref. [24] for (a) ethanol in solution and (b) paraffin in gas phase.

In conclusion, nonlinear spatiotemporal dynamics in graded-index multimode fibers open the possibility to generate visible to mid-infrared supercontinuum via dedicated fiber cascades. We have developed an easy-to-implement supercontinuum source that can be pumped by commercial lasers. With this technique, we have created the first three-octave spanning supercontinuum source, covering the spectral range from 0.75 to 6 μm . We have illustrated the potential of this source in the detection of organic compounds by molecular absorption spectroscopy. We believe that the use of chalcogenide glass fibers based on heavier atoms (such as Se) will increase the spectral coverage to cover the entire molecular fingerprint region, up to 12 μm . Such improvements in supercontinuum sources are expected to benefit applications requiring both spatial coherence and average power, such as infrared spectromicroscopy [11] and optical coherence tomography [25].

Funding. Conseil Régional Aquitaine (MIR-X, SCIR, SIP2); Agence Nationale de la Recherche (ANR-16-CE08-0031 BISCOT, ANR-21-CE24-0001 MIRthFUL).

Disclosures. The authors declare no conflicts of interest.

Data availability. Data underlying the results presented in this paper are not publicly available at this time but may be obtained from the authors upon reasonable request.

REFERENCES

1. H. A. Bechtel, E. A. Muller, R. L. Olmon, M. C. Martin, and M. B. Raschke, *Proc. Natl. Acad. Sci.* **111**, 7191 (2014).

2. M. C. Martin and P. Dumas, in *Spectroscopic Properties of Inorganic and Organometallic Compounds*, Vol. 43, J. Yarwood, R. Douthwaite, and S. Duckett, eds. (Royal Society of Chemistry, 2012), pp. 141.
3. U. Willer, M. Saraji, A. Khorsandi, P. Geiser, and W. Schade, *Opt. Lasers Eng.* **44**, 699 (2006).
4. R. Croce and H. Van Amerongen, *Science* **369**, eaay2058 (2020).
5. M. Y. Sfeir, F. Wang, L. Huang, C.-C. Chuang, J. Hone, S. P. O'Brien, T. F. Heinz, and L. E. Brus, *Science* **306**, 1540 (2004).
6. C. Guo, F. I. Allen, Y. Lee, T. P. Le, C. Song, J. Ciston, A. M. Minor, and E. D. Gomez, *Adv. Funct. Mater.* **25**, 6071 (2015).
7. H.-Y. N. Holman, H. A. Bechtel, Z. Hao, and M. C. Martin, *Anal. Chem.* **82**, 8757 (2010).
8. C. Bauer, A. K. Sharma, U. Willer, J. Burgmeier, B. Braunschweig, W. Schade, S. Blaser, L. Hvozdar, A. Müller, and G. Holl, *Appl. Phys. B* **92**, 327 (2008).
9. P. Patapis, E. Nasedkin, G. Cugno, A. M. Glauser, I. Argyriou, N. P. Whiteford, P. Mollière, A. Glasse, and S. P. Quanz, *Astron. Astrophys.* **658**, A72 (2022).
10. O. Venot, B. Drummond, Y. Miguel, I. P. Waldmann, E. Pascale, and T. Zingales, *Exp. Astron.* **46**, 101 (2018).
11. F. Borondics, M. Jossent, C. Sandt, L. Lavoute, D. Gaponov, A. Hideur, P. Dumas, and S. Février, *Optica* **5**, 378 (2018).
12. S. Venck, F. St-Hilaire, L. Brilland, A. N. Ghosh, R. Chahal, C. Cailaud, M. Meneghetti, J. Troles, F. Joulain, S. Cozic, S. Poulain, G. Huss, M. Rochette, J. M. Dudley, and T. Sylvestre, *Laser Photonics Rev.* **14**, 2000011 (2020).
13. Y. Leventoux, G. Granger, K. Krupa, T. Mansuryan, M. Fabert, A. Tonello, S. Wabnitz, V. Couderc, and S. Février, *Opt. Lett.* **46**, 3717 (2021).
14. L. G. Wright, D. N. Christodoulides, and F. W. Wise, *Nat. Photonics* **9**, 306 (2015).
15. K. Krupa, A. Tonello, A. Barthélémy, V. Couderc, B. M. Shalaby, A. Bendahmane, G. Millot, and S. Wabnitz, *Phys. Rev. Lett.* **116**, 183901 (2016).
16. K. Krupa, C. Louot, V. Couderc, M. Fabert, R. Guenard, B. M. Shalaby, A. Tonello, D. Pagnoux, P. Leproux, A. Bendahmane, R. Dupiol, G. Millot, and S. Wabnitz, *Opt. Lett.* **41**, 5785 (2016).
17. Z. Liu, L. G. Wright, D. N. Christodoulides, and F. W. Wise, *Opt. Lett.* **41**, 3675 (2016).
18. K. Krupa, A. Tonello, B. M. Shalaby, M. Fabert, A. Barthélémy, G. Millot, S. Wabnitz, and V. Couderc, *Nat. Photonics* **11**, 237 (2017).
19. K. Krupa, A. Tonello, A. Barthélémy, T. Mansuryan, V. Couderc, G. Millot, P. Grelu, D. Modotto, S. A. Babin, and S. Wabnitz, *APL Photonics* **4**, 110901 (2019).
20. L. G. Wright, Z. Liu, D. A. Nolan, M.-J. Li, D. N. Christodoulides, and F. W. Wise, *Nat. Photonics* **10**, 771 (2016).
21. S. H. Baek and W. B. Roh, *Opt. Lett.* **29**, 153 (2004).
22. N. B. Terry, T. G. Alley, and T. H. Russell, *Opt. Express* **15**, 17509 (2007).
23. M. Conforti, C. Mas Arabi, A. Mussot, and A. Kudlinski, *Opt. Lett.* **42**, 4004 (2017).
24. K. Huber and G. Herzberg, *NIST chemistry webbook*, NIST Standard Reference Database Number 69 (National Institutes of Standards and Technology, 2005).
25. M. Maria, I. Bravo Gonzalo, T. Feuchter, M. Denninger, P. M. Moselund, L. Leick, O. Bang, and A. Podoleanu, *Opt. Lett.* **42**, 4744 (2017).

